Rare-Earth-Compound Nanowires, Nanotubes, and Fullerene-Like Nanoparticles: Synthesis, Characterization, and Properties

Xun Wang and Yadong Li*[a]

Abstract: Various low-dimensional nanostructures, such as nanowires, nanotubes, nanosheets, and fullerene-like nanoparticles have been selectively synthesized from rare-earth compounds (hydroxides, fluorides) based on a facile hydrothermal method. The subsequent dehydration, sulfidation, and fluoridation processes lead to the formation of rare-earth oxide, oxysulfide, and oxyhalide nanostructures, which can be functionalized further by doping with other rare-earth ions or by coating with metal nanoparticles. Owing to the interesting combination of novel nanostructures and functional compounds, these nanostructures can be expected to bring new opportunities in the vast research areas of and application in biology, catalysts, and optoelectronic devices.

Keywords: actinides · inorganic fullerenes · lanthanides · layered compounds · nanostructures

Introduction

Recent years have seen considerable interest in the fabrication of low-dimensional nanosized materials, such as nanowires, nanotubes, nanobelts, and inorganic fullerene-like (IF) nanoparticles.[1–5] These systems, with at least one restricted dimension, may offer opportunities for investigating the influence of shape and dimensionality on optical, magnetic, and electronic properties. They may furthermore be of great application value for their novel properties induced by such reduced dimensionalities. Up to now, many kinds of novel nanostructures have been successfully synthesized, such as III-V[6–9] and II-VI semiconductors,[10–17] elemental and oxide nanowires/nanorods,[18–26] MX_2 (M = Mo, W; X = S, Se) nanotubes and IF nanoparticles,[27–30] and semiconducting oxide nanobelts,[31–33] amongst others. However, owing to the lack of understanding of the general principles of the controlled synthetic processes, the synthesis of nanostructures with designated well-confined dimensionality and size remains a challenge. Herein we will report on the controlled synthesis of a new class of novel nanostructures: nanowires, nanotubes and IF nanoparticles from rare-earth compounds (hydroxides, oxides, oxysulfides, oxyhalides), based on a hydrothermal synthetic pathway; their thermal stability, further functionalization, and other properties have also been investigated.Rare-earth compounds have drawn continuous research attention for many years because of their unique optical, catalytic, and magnetic properties. These compounds have been widely used in various fields, such as high-quality phosphors, up-conversion materials, catalysts, and so forth.[34] Most of these useful functions originate from the electron transitions within the 4f shell, and are highly sensitive to the composition and structures of the rare-earth compounds, especially to the complexation state and the crystal field of the matrix in which rare-earth ions are trapped.[35] Of special interest is the technique whereby rare-earth ions are introduced into well-defined porous nanostructures.[36–38] Energy can be transferred to rare-earth ions more effectively in this way, so that they will show enhanced optical and magnetic properties. However, the relative poor thermal stability of the porous structures, induced by the utilization of structure-directing reagents, still remains as a challenge in the production of such materials.Recently, we have developed a facile hydrothermal synthetic pathway for the production of lanthanide hydroxide nanowires.[24] Further studies showed that, under lower temperature and appropriate pH conditions, nanotubes and IF nanoparticles of rare-earth hydroxides could also be obtained. A similar procedure has been applied in the synthesis of rare-earth fluoride IF nanoparticles.[39] Due to their particularly interesting structures, these materials should be of great research and application interest. In this paper, a systematic study has been carried out to investigate the controlled formation of nanowires, nanosheets, nanotubes, and IF nanoparticles as well as their thermal stability, further functionalization, and other properties.Our synthesis is based on the preparation of rare-earth hydroxide (or fluoride) colloidal precipitates at room tem-

[a] Prof. Y. Li, X. Wang
Department of Chemistry, Key Laboratory of Atomic and Molecular Nanosciences (Ministry of Education, China)
Tsinghua University, Beijing, 100084 (P. R. China)
Fax: (+86) 10-62788765
E-mail: ydli@tsinghua.edu.cn

 DOI: 10.1002/chem.200304785

perature, and the subsequent hydrothermal treatment at designated temperature and pH conditions. By controlling the temperature and pH in solution, hydroxide nanowires, nanosheets, and nanotubes could be selectively synthesized. With these hydroxides as precursors, the subsequent dehydration, sulfuration, and fluoridation processes lead to the formation of rare-earth oxide, oxysulfide, and oxyfluoride nanowires, nanosheets, and nanotubes. Owing to the excellent hydrophilicity, thermal stability, and novel properties of the rare-earth compounds, these nanostructures may find applications in, amongst others, biological and catalytic fields

Results and Discussion

Nanowires, nanotubes and IF nanostructures of hexagonal rare-earth hydroxides and fluorides obtained by a precipitation-hydrothermal synthetic pathway

Rare-earth hydroxide nanowires and nanotubes: The synthesis of hydroxide nanowires and nanotubes were based on the preparation of colloidal hydroxide precipitates at room temperature, and the subsequent hydrothermal treatment at 120–180 °C for 12–24 hours (Scheme 1).

The hydrothermal method was shown to be effective in the synthesis of one-dimensional nanostructures such as

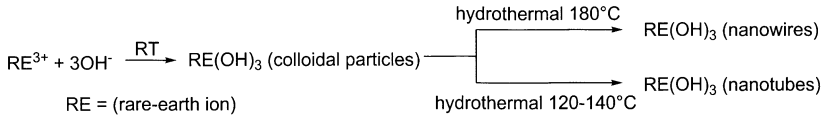

Scheme 1.

MnO_2 nanowires,[22–23] and bismuth[25] and titanate nanotubes.[33]. By the simply tuning of factors such as pH, temperature, and concentration, the experimental conditions could be chosen to favor the anisotropic growth of materials. In our experiments, nanowires/nanorods of rare-earth hydroxides ($Y(OH)_3$, $La(OH)_3$, $Pr(OH)_3$, $Nd(OH)_3$, $Sm(OH)_3$, $Eu(OH)_3$, $Gd(OH)_3$, $Tb(OH)_3$, $Dy(OH)_3$, $Ho(OH)_3$, $Er(OH)_3$, $Tm(OH)_3$, YbOOH) with different aspect ratios were successfully obtained under the higher-temperature conditions (180 °C) through this precipitation–hydrothermal synthetic method.Temperature, pH, and the crystal structures have been found to be responsible for the growth of rare-earth hydroxide nanowires.By altering the pH in the solution, nanowires of the hydroxides with different aspect ratios were obtained. TEM images of $La(OH)_3$ nanorods ($pH \approx 10$) and nanowires (KOH concentration 5 mol l^{-1}) are shown in Figure 1a and 1b, respectively. Electron diffraction (ED) and HRTEM analysis have shown that they are single crystals, and in most cases the growth direction is along the [0 0 1] axis.The crystal structures of the hydroxides may be the inherent factor that will determine their growth behavior. X-ray diffraction (XRD) characterization has shown that most of the rare-earth hydroxides obtained under these

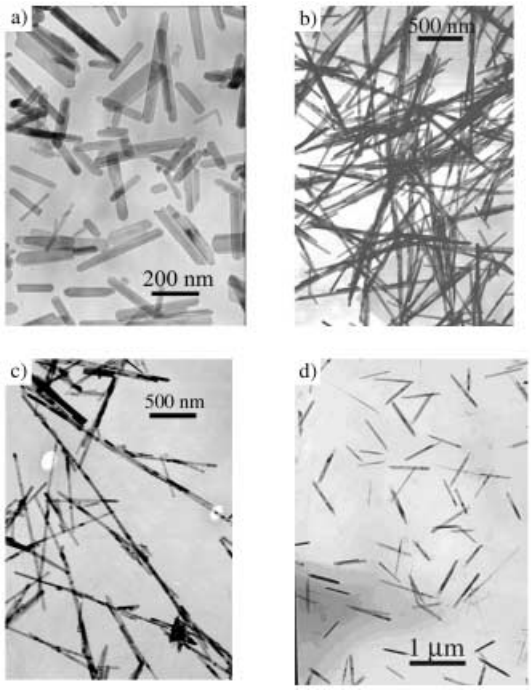

Figure 1. a) TEM image of $La(OH)_3$ nanorods (180 °C, $pH \approx 10$); b) TEM image of $La(OH)_3$ nanowires (180 °C, KOH concentration 5 mol L^{-1}); c) TEM image of $Pr(OH)_3$ nanowires (180 °C, KOH concentration 5 mol L^{-1}); d) TEM image of $Y(OH)_3$ nanorods (180 °C, $pH \approx 13$).

experimental conditions have hexagonal structures. As an example, Figure 2 shows the reflection patterns of $Dy(OH)_3$ (Figure 2a) and $Eu(OH)_3$ (Figure 2b), which could be readily indexed to that of the hexagonal phase of $Dy(OH)_3$ and $Eu(OH)_3$. With decreasing ion radius, the peaks in the hexagonal phase gradually shift to smaller *d* values (Figure 2 inset). In the case of Yb, the monoclinic phase of YbOOH (Figure 3b) is obtained instead of the hexagonal phase of $Yb(OH)_3$ (Figure 3a). Correspondingly, TEM characterization shows that the nanowire products, produced under exactly the same conditions, become less uniform in the series

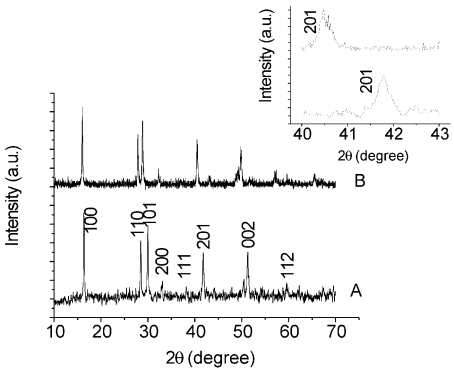

Figure 2. A) XRD patterns of $Dy(OH)_3$ nanowires (180 °C, $pH \approx 13$); B) XRD patterns of $Eu(OH)_3$ nanowires (180 °C, $pH \approx 13$).

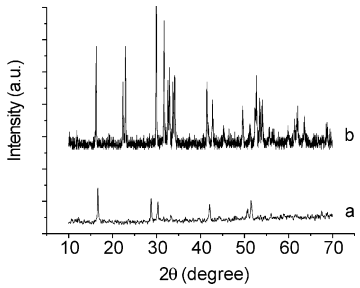

Figure 3. a) XRD patterns of hexagonal $Yb(OH)_3$ nanotubes (140 °C, pH ≈ 13); b) XRD patterns of monoclinic YbOOH (180 °C, KOH concentration 5 mol L^{-1}).

from $La(OH)_3$ to YbOOH; this may mean that the anisotropic growth tendency has been weakened to some extent. As an analogy to the lanthanide hydroxides, $Y(OH)_3$ has a similar hexagonal crystal structure, and could be prepared as uniform nanowires (Figure 1d, 180 °C, pH ≈ 13). Based on our experimental results, it seems reasonable to imagine that the driving force for the growth of nanowires could be attributed to their crystal structures.It is interesting to find that at an optimal pH condition of ≈13 (temperature = 180 °C), $Er(OH)_3$ and $Y(OH)_3$ nanotubes have been found to coexist with nanorods and nanosheets in the final products. Furthermore, in the optimization process to get rare-earth hydroxide nanowires, the hydroxides could be prepared as uniform nanosheets (Figure 4a) in a certain pH range. All these clues indicate that nanotubes of rare-earth hydroxides could be obtained under appropriate conditions. This seems reasonable, since the rare-earth hydroxides have hexagonal layered structures, just like those of most of the reported nanotubes.[33,40] This hypothesis has been confirmed by a series of experiments carried out at a lower temperature of 120–140 °C and a controlled pH of ≈13. Rare-earth hydroxide (from Y, La to Yb) nanotubes were obtained. Considering that the pathways to the formation of rare-earth nanowires and nanotubes only differ in temperature, nanowires can be the thermodynamically stable form of nanotubes.Similar to the nanowire products, hexagonal structures were found for all the obtained nanotube products ($Y(OH)_3$, $La(OH)_3$, $Pr(OH)_3$, $Nd(OH)_3$, $Sm(OH)_3$, $Eu(OH)_3$, $Gd(OH)_3$, $Tb(OH)_3$, $Dy(OH)_3$, $Ho(OH)_3$, $Er(OH)_3$, $Tm(OH)_3$, $Yb(OH)_3$). Dehydration of $Yb(OH)_3$ to yield YbOOH will occur when the temperature is increased to around 180 °C. As shown in Figure 3a, the reflection patterns could be readily indexed to that of the hexagonal phase of $Yb(OH)_3$.It is interesting to find that, under similar experimental conditions, light lanthanide hydroxides could be prepared as nanotubes with smaller diameters, while those of heavy lanthanide hydroxides possessed larger diameters (Figure 4d–g). This can be attributed to the gradual changes of the ion radii of the rare-earth ions. Generally speaking, nanotubes of $Y(OH)_3$, $Yb(OH)_3$, $Tm(OH)_3$, $Er(OH)_3$, $Ho(OH)_3$, $Dy(OH)_3$, and $Tb(OH)_3$ have diameters from around tens of nanometers to more than one hundred nanometers, while those of $Gd(OH)_3$ ($Gd(OH)_3$, $Eu(OH)_3$, $Sm(OH)_3$, $Nd(OH)_3$, $Pr(OH)_3$, $La(OH)_3$) usually have diameters less than twenty nanometers (Figure 4h). It is worth noting that all these nanotubes have open ends; this may provide the possibility for subsequent functionalization of their inner surface. Figure 4f shows a typical image of a $Dy(OH)_3$ nanotube with an open end. HRTEM analysis indicates the multiwalled structures of these nanotubes

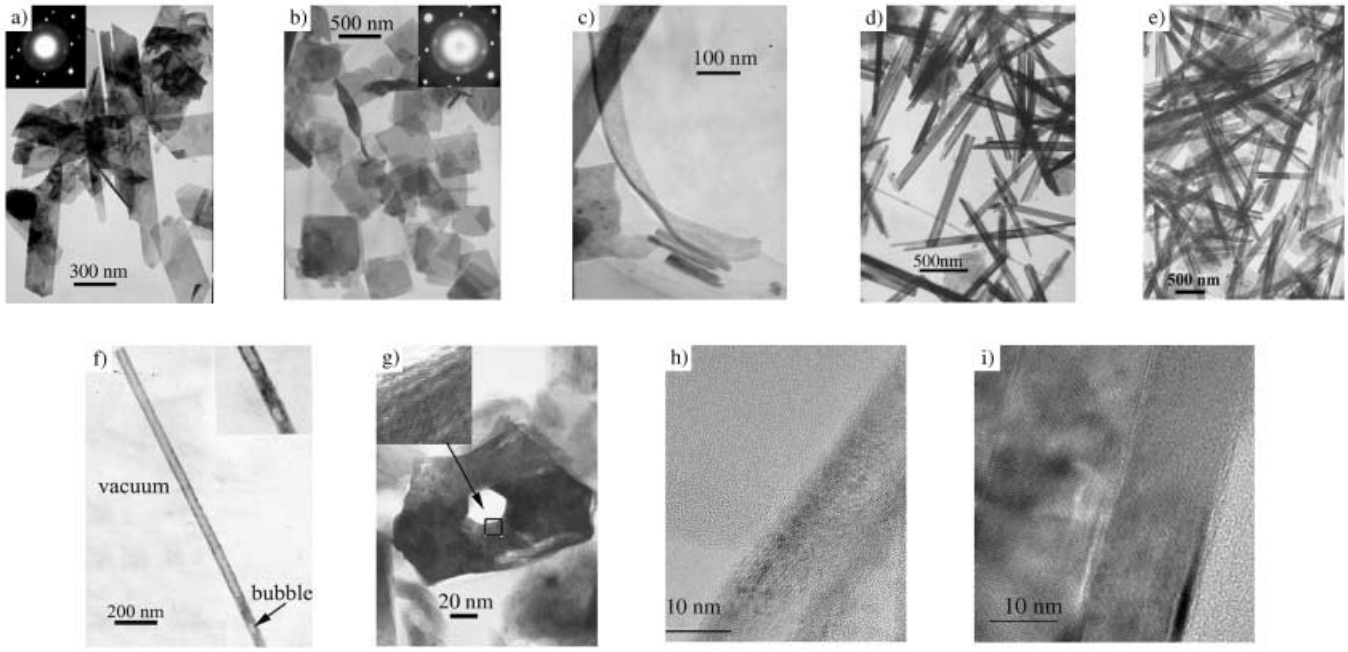

Figure 4. a) Nanosheets of $Sm(OH)_3$ (180 °C, pH 6–7); b) nanosheets of $Er(OH)_3$ (140 °C, pH ≈ 10); c) individual nanobelts of $Er(OH)_3$ (140 °C, pH ≈ 7); d) nanotubes of $Yb(OH)_3$ (120 °C, pH ≈ 13); e) nanotubes of $Tm(OH)_3$ (140 °C, pH ≈ 13); f) individual nanotube of $Dy(OH)_3$ (120 °C, pH ≈ 13), inset shows an air bubble trapped in the nanotube and the meniscus indicates excellent hydrophilicity; g) cross section of an individual $Er(OH)_3$ nanotube; h) HRTEM image of $Eu(OH)_3$ nanotubes; i) HRTEM image of individual $Dy(OH)_3$ nanotube.

(Figure 4g–i). The interlayer spacing in Figure 4i has been calculated to be about 0.35 nm, approximately the separation between (001) planes of $Dy(OH)_3$. A HRTEM image of the cross section of an individual $Er(OH)_3$ nanotube has been provided in Figure 4g, from which the inner and outer diameter can be calculated to be $\approx$30 nm and $\approx$100 nm, respectively.Besides temperature, pH plays an important role in the synthesis of rare-earth hydroxide nanotubes. This was investigated during the synthesis of $Er(OH)_3$ nanotubes. Nanosheets (Figure 4b) were found to be the main products in the lower pH range (7–10). This provided evidence of the two-dimensional growth tendency of these hydroxides. Once the nanosheets formed, they cannot be transformed into nanotubes if treated at higher pH conditions. This is due to the existence of an energy barrier going from rigid lamellar structures to nanotubes. ED analysis showed their single crystal nature, which was indexed to a hexagonal phase with the [001] axis parallel to the electron beam. When the pH was kept at $\approx$7, nanobelts of $Er(OH)_3$ were obtained (Figure 4c). These nanosheets and nanobelts usually are electron sensitive, and will curl from the edge under electron bombardment, indicating a possible rolling process for the formation of the nanotubes . At a pH range of 12–13, nanotubes of $Er(OH)_3$ were found in the final products.The above experiments show that appropriate temperature and pH conditions will favor the formation of hydroxide nanosheets, and the as-obtained nanosheets could serve as precursors for hydroxide nanotubes. As far as the colloidal precipitates are concerned, the optimal conditions for the formation of nanotubes are a basic environment. However, if these oxides were not dissolved in diluted acid, but dispersed into deionized water and directly treated at 120–180 °C, a small amount of nanotubes and fullerene-like nanoparticles could be occasionally observed in the obtained samples (Scheme 2).

$$RE_2O_3 + H_2O \xrightarrow{\text{hydrothermal } 180^\circ C} RE(OH)_3 \text{ (nanotubes, IF nanoparticles)}$$

Scheme 2.

The reactions between most of the rare-earth oxides and water can occur spontaneously. However, this usually results in irregular microparticles. Under controlled hydrothermal conditions, they may be gradually exfoliated into hydroxide nanosheets, and then grow into nanotubes.From our experimental results, the oxides of La, Pr, Nd, Sm, Eu, Gd, and Tb were completely transformed into hydroxides in the temperature range 120–180 °C. The oxides of Dy and Y were only transformed into hydroxides in the range 160–180 °C (Figure 5). The mixed phase of oxides and hydroxides of Ho, Er, Tm, and Yb were obtained in the adopted temperature range.Nanotubes of hydroxides were observed in the products of $Y(OH)_3$, $Sm(OH)_3$, $Eu(OH)_3$ (Figure 6a), $Gd(OH)_3$ (Figure 6b), $Tb(OH)_3$, and $Dy(OH)_3$. Nanotubes also exist in the Ho, Er, Tm, and Yb products, although the XRD characterization shows that the final products are not pure hydroxides. Considering that the oxides do not have layered structures and the experimental conditions are similar to that of other hydroxides, it would be reasonable to conclude that these nanotubes are hydroxide nanotubes. ED analysis taken from a single nanotube of $Er(OH)_3$ indicate its hexagonal symmetry and the growth direction along the [010] axis. A typical image of $Eu(OH)_3$ nanotubes is shown in Figure 6a, from which it can be seen that they stem from aggregates of microparticles. Although nanotubes can be obtained through this conversion method, thorough TEM investigations of the products showed most of the obtained hydroxides remain as irregular microparticles (yield of nanotubes $<10\%$).Fullerene-like hydroxide nanoparticles (Figure 7c, $Eu(OH)_3$ IF nanoparticles) were found to coexist with nanotubes. Different from nanotubes, the formation of IF nanoparticles requires folding in all directions, and thus involves a higher elastic strain. Generally, the synthesis of IF nanoparticles does not need a catalyst, but usually requires relatively high temperatures. However, in this oxide conversion method, it seems that the forced hydration and gradual exfoliation process provided the energy needed for the formation of IF nanoparticles.Similar exfoliation process exists in the titanate system, and the exfoliation of TiO_2 powders into macromolecular-like nanosheets in solution has been demonstrated by T. Sasaki et al.[40] Further studies showed that nanotubes of titanate could be obtained through hydrothermal treatment of TiO_2 in basic solution.[33] Most of the rare-earth hydroxides have hexagonal layer structures, which provided the possibility for their exfoliation and further rolling into nanotubes or IF nanostructures.

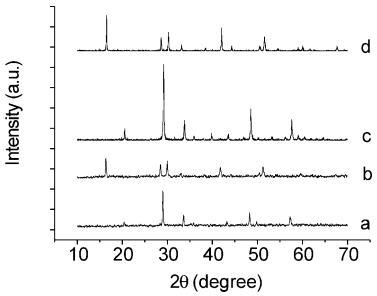

Figure 5. a) XRD patterns of Dy_2O_3 (140 °C, 48 h); b) XRD patterns of $Dy(OH)_3$ (180 °C, 48 h); c) XRD patterns of Y_2O_3 (140 °C, 48 h); d) XRD patterns of $Y(OH)_3$ (180 °C, 48 h).

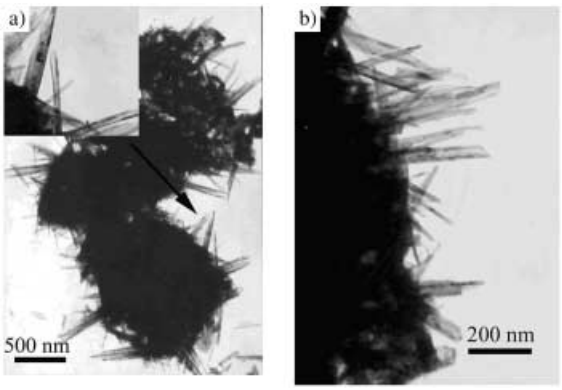

Figure 6. a) TEM image of $Eu(OH)_3$ nanotubes; b) TEM image of $Gd(OH)_3$ nanotubes.

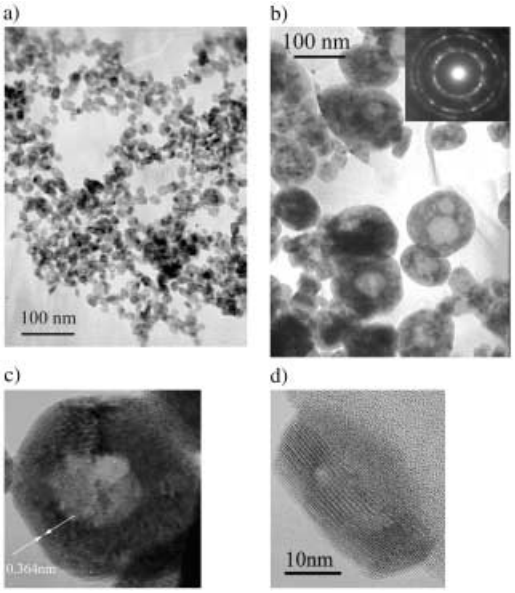

Figure 7. a) TEM image of PrF_3 (120 °C, Pr^{3+}:NH_4F = 1:3 (mole ratio), pH 4–5); b) TEM image of PrF_3 IF nanoparticle with diameter ≈100 nm (180 °C, Pr^{3+}:NH_4F = 1:3 (mole ratio), pH 4–5); c) HRTEM image of an individual $Eu(OH)_3$ IF nanoparticle with diameter ≈45 nm; d) HRTEM image of an individual LaF_3 IF nanoparticle.

Although the exact formation mechanism for the conversion of rare-earth oxide particles into hydroxide nanotubes remains unknown, it seems an effective way to get IF and nanotubes structures.

Formation of rare-earth fluoride IF nanoparticle: Similar precipitation–hydrothermal methods have been applied in the synthesis of rare-earth fluoride IF nanoparticles. In a typical synthesis, the fluoride colloidal nanoparticles were hydrothermally treated at a temperature range of 80–180 °C (Scheme 3).

$$RE^{3+} + F^- \xrightarrow{\text{adjust pH}} \text{colloidal particles} \xrightarrow{\text{hydrothermal 180°C}} \text{IF nanoparticles}$$

Scheme 3.

The formation of IF nanoparticles seems to be related to the hexagonal structures, since IF nanoparticles were only found in the samples of lanthanide fluorides that possessed hexagonal crystal structures: LaF_3, PrF_3, NdF_3, and SmF_3. In the orthorhombic YF_3, less IF nanoparticles were observed.-Due to the difference in K_{sp}, the final products were characterized to be rare-earth fluorides until the pH of the system was adjusted to about 10. When the pH was kept above 12, pure-phase hydroxide nanowires were obtained.The sizes of these nanoparticles have shown a fairly large distribution. Figure 7 shows a series of fullerene-like nanoparticles with sizes ranging from 10 nm to more than 100 nm, which were obtained from a temperature of 120 and 180 °C, respectively.HRTEM analysis (Figure 7d) shows that the obtained LaF_3 nanoparticles have close-caged structures. The interlayer spacing can be calculated to be ≈0.36 nm (the approximate separation between (002) planes of LaF_3), and electron diffraction patterns, taken from a single nanoparticle, revealed its single-crystal nature.For the first time, fullerene-like nanoparticles were successfully prepared from fluorides and hydroxides; this has greatly extended the scope of IF nanostructures.Although nanotubes were not obtained under current experimental conditions, we believe that the nanotubes also exist for these fluorides.

Our study shows, based on this facile hydrothermal synthetic pathway, that all kinds of nanostructures of rare-earth compounds could be prepared. We believe that the exact formation mechanism for the controlled growth of nanowires, nanotubes, and IF nanoparticles in solution deserves further study, and that this hydrothermal solution route may be developed to be a general, controllable synthetic method.

Conversion of hydroxides into oxides, oxyfluorides, and oxysulfides: With the above hydroxides as possible precursors, oxide, oxyfluoride, and oxysulfide nanowires, nanotubes, or nanosheets were easily obtained by the following dehydration, fluoridation and/or sulfidation processes (Scheme 4).

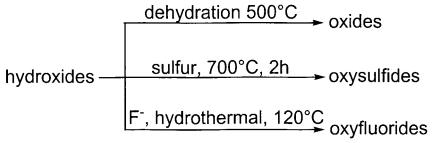

Scheme 4.

Although the crystal structures changed after these treatments, the morphologies were maintained, perhaps due to the higher activation energies needed for the collapse of these nanostructures. The hydroxides can be converted into oxides after thermal treatment at 500 °C for two hours.Figure 8 shows the TGA-DTA curve of the $Sm(OH)_3$ nanowires. The DTA curve shows two peaks at ≈300 and 420 °C, indicating a two step dehydration process, which corresponds to the transformation process of $Sm(OH)_3 \rightarrow SmOOH \rightarrow Sm_2O_3$. A similar dehydration process exists in the transformation from the rare-earth hydroxide to oxide nanostructures. TEM characterization shows that the nanowire morphologies of La_2O_3 were mantained, even after thermal treatment at 600 °C for two hours (Figure 9a).A process for the sulfidation of rare-earth hydroxides into oxysulfides was developed by mixing the sulfur and hydroxide nanostructures together, followed by the subsequent thermal

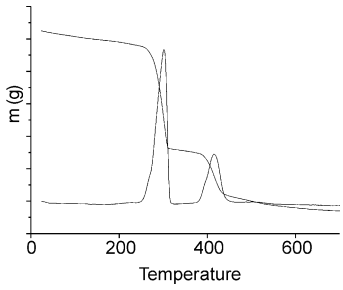

Figure 8. TGA–DTA curve of the $Sm(OH)_3$ nanowires.

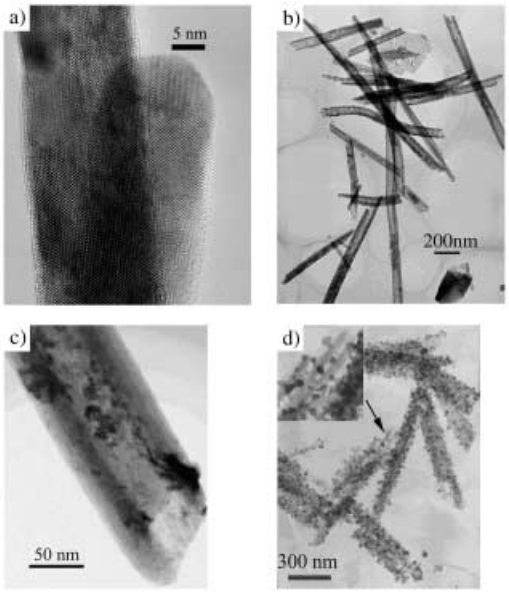

Figure 9. a) HRTEM image of La_2O_3 nanowires; b) TEM image of Y_2O_2S nanotubes; c) TEM image of individual Y_2O_2S nanotube with an open end; d) TEM image of $Y(OH)_3$ nanotubes coated with Au nanoparticles.

treatment at 700 °C under a protective Ar (or N_2) atmosphere for approximately two hours. As an example, the reflection patterns in Figure 10c could be readily indexed to the hexagonal phase of Y_2O_2S. Even after thermal treatment, the morphologies of these nanostructures could be maintained (Figure 9b,c). HRTEM analysis shows that the hydroxide single-crystal nanotubes were transformed into crystalline nanotubes. The broadening of the peaks in Figure 10c indicates smaller crystal sizes than in the hydroxide precursors, as was also observed in the oxide transformation process (Figure 10b). Based on the above studies it was evident that these nanostructures are stable under thermal treatment, which may be rather useful for their applications in catalyst fields.The hydroxides could also be converted into oxyhalides if the hydroxides were re-dispersed into solutions that contained halide ions, and re-treated at approximately 120 °C for about 12 hours. Oxyfluoride nanorods and nanotubes were easily obtained by following this process, and ED analysis proved that the single-crystal nature of the as-obtained nanostructures was maintained. From the XRD patterns in Figure 10d, we noted that the hexagonal crystal

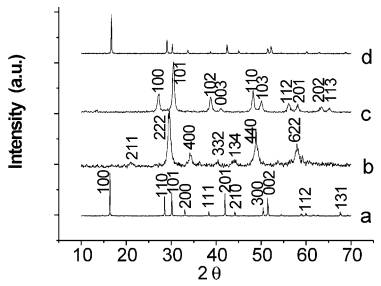

Figure 10. XRD patterns of a) $Y(OH)_3$; b) Y_2O_3; c) Y_2O_2S; d) $Y(OH)_{2.14}F_{0.86}$.

structures did not change with respect to the hydroxide precursors. However, the main peaks shifted to smaller *d* values (Figure 10a, d).Many other transformation modes exist to obtain rare-earth compound 1D nanostructures. Since the novel properties of the rare-earth compounds depend greatly on the crystal field in which the rare-earth ions are trapped, these conversions will greatly enrich the accessible classes of materials.

Functionalization of the as-obtained rare-earth nanostructures: By simply co-dissolving the target ions with the oxides, and followed by the routine procedures, the above nanostructures could be easily functionalized. Since the rare-earth hydroxides have similar crystal structures, lattice mismatch was no serious concern, and homogenously doped nanostructures could be easily obtained.The unique inner and outer surface of the nanotubes make them possible candidates for many potential applications, for example, as effective templates for the growth of new types of 1D nanostructures and/or nanocomposites, or as support for catalysts.Au–$Y(OH)_3$ nanotube composites were synthesized by the following procedure. $Y(OH)_3$ nanotubes were dispersed into aqueous hydrazine solution through ultrasonic treatment. As a result, aqueous hydrazine was absorbed onto the outer and/or inner surface of the tubes. After filtration the nanotubes were dispersed into solutions of Au^{3+} (or Ag^+, etc.). The Au^{3+} ions would be reduced in situ by the aqueous hydrazine, leading to nanotubes coated with Au (or Ag, etc.) nanoparticles (Figure 9d).Functionalized nanostructures of oxides, oxysulfides, and oxyhalides could also be prepared with the functionalized hydroxides as precursors. As an example, Eu-doped and Yb–Er co-doped Y_2O_2S nanotubes have been synthesized. $Y(OH)_3$ nanotubes were first dispersed into aqueous solutions ($0.04\ mol\,L^{-1}$) of Eu^{3+} or Yb^{3+}/Er^{3+} (Er:Yb = 1:6), then stirred for two hours, filtered, and dried at 80 °C. After a sulfidation process, the doped $Y(OH)_3$ nanotubes could be converted into doped oxysulfide nanotubes. Yb and Er-codoped Y_2O_2S is an efficient near-IR-to-visible up-conversion material, in which Yb acts as an absorber and Er as an emitter in the crystal lattice. When excited by a 980 nm IR light, the absorber in the phosphor absorbs the light and transfers the energy to the emitter, which emits visible light. In a typical Yb/Er up-conversion system, Yb absorb energy and forms a transition state, which then transfers its energy to Er (Figure 11a). A strong up-conversion emission under illumination by ordinary Xe sources (excitation wavelength: 980 nm) was observed (Figure 11c) in the Yb^{3+} and Er^{3+} co-doped Y_2O_2S nanotubes. Emission bands centered at 650 nm (due to the electron transition from $^4F_{9/2}$ to $^4I_{15/2}$ levels) and 730 nm (due to the electron transition from $^4I_{9/2}$ to $^4I_{15/2}$ levels) coincide well with the down-conversion emission (two bands, 500 nm and 730 nm) of these nanotubes when excited with 300, 310, or 320 nm Xe sources (Figure 11b). It is also interesting to find that the intensity of the up-conversion luminescence is linearly proportional to the excitation intensity (Figure 11c, inset). Although the exact reasons for this remain unknown, it may be due to the particular nanotube morphology of the samples.Up-conversion phenomena have also been observed

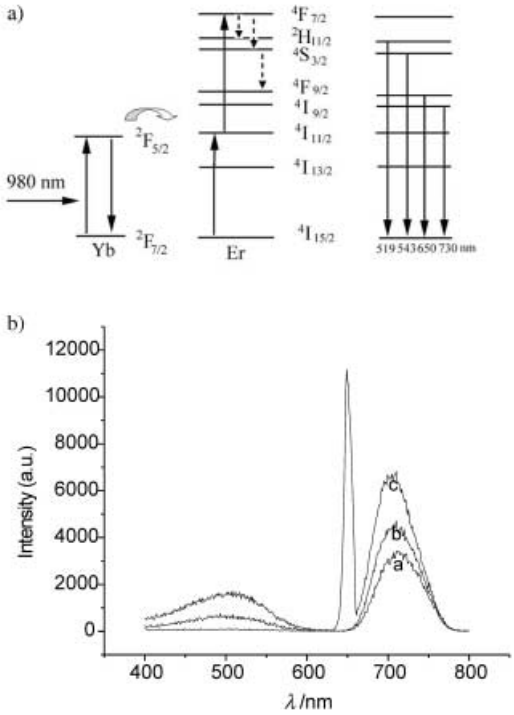

Figure 11. a) Electronic energy-level diagram for Yb and Er ions and a schematic illustration of two excitation process. b) Down-conversion spectrum of Yb^{3+}/Er^{3+} co-doped Y_2O_2S nanotubes (Xe sources, 300 nm (a), 310 nm (b), 320 nm (c)). c) Up-conversion spectrum of Yb^{3+}/Er^{3+} co-doped Y_2O_2S nanotubes (Xe sources, 980 nm); inset: curve of excitation intensity versus emission intensity.

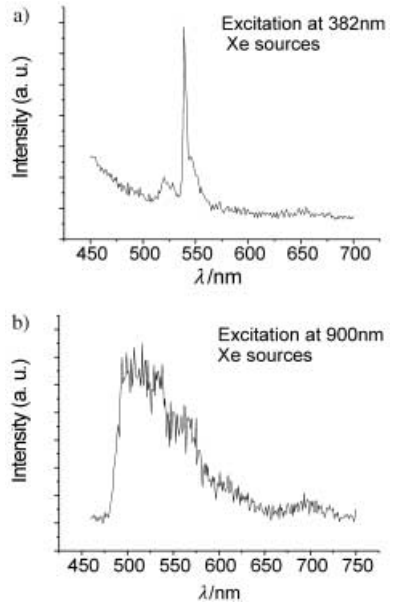

Figure 12. a) Down-conversion spectrum of Yb^{3+}/Er^{3+} co-doped LaF_3 IF nanoparticles (Xe sources, 310 nm). b) Up-conversion spectrum of Yb^{3+}/Er^{3+} co-doped LaF_3 IF nanoparticles (Xe sources, 900 nm).

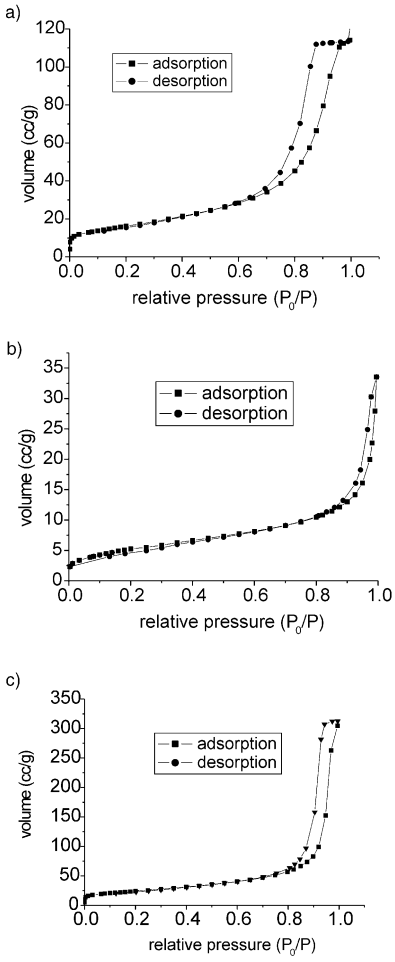

Figure 13. N_2 adsorption–desorption isotherm of a) PrF_3 IF nanoparticles (120 °C, average diameter, 10 nm); b) $Y(OH)_3$ nanotubes (average diameter ≈100 nm, length 2—4 μm); c) $La(OH)_3$ nanorods (diameter 5≈10 nm, lengths 50≈100 nm).

in the Yb^{3+}–Er^{3+} co-doped fluoride IF nanoparticles (Figure 12). However, due to the changes of host materials and the subsequent changes of the crystal field, the up-conversion and the down-conversion bands shifted to about 520–540 nm (corresponding to electron transition from $^2H_{11/2}$ and $^4S_{3/2}$ to $^4I_{15/2}$, respectively).Since rare-earth compounds have wide applications in catalysis, Brunauer–Emmet–Teller (BET) analysis was used to characterize these nanostructures.Nitrogen adsorption–desorption isotherms of PrF_3 IF nanoparticles, $Y(OH)_3$ nanotubes, and $La(OH)_3$ nanowires are shown in Figure 13. These isotherms can be categorized

as type IV with a distinct hysteresis loop. The BET surface-area data, 58.03 $m^2 g^{-1}$ (Figure 13a) for PrF_3 IF nanoparticles (120 °C, average diameter: about 10 nm) and 19.78 $m^2 g^{-1}$ (Figure 13b) for $Y(OH)_3$ nanotubes (average diameter $\approx$ 100 nm and length 2–4 μm), are much larger than the calculated value for the monodispersed PrF_3 nanoparticles (43.92 $m^2 g^{-1}$ for 10 nm particles, density of a single crystal of PrF_3: 6.83 $g cm^{-3}$) and $Y(OH)_3$ nanorods (less than 10 $m^2 g^{-1}$), indicating their hollow and tubular characteristics. The BET surface data for $La(OH)_3$ nanorods (diameter 5–10 nm, length 50–100 nm) was calculated to be 84.95 $m^2 g^{-1}$ (Figure 13c), satisfactory for potential applications in surface catalysis fields.Further studies are being performed concerning the novel properties and exploration for application of these nanostructures, such as catalytic, optoelectronic, magnetic, biological, and luminescence properties. It is foreseeable that these novel low-dimensional functional nanostructures with different shapes and sizes will provide further research opportunities in chemistry, physics, and other interdisciplinary fields of science and technology.

Conclusion

Based on a facile hydrothermal method, various nanostructures such as nanowires, nanotubes, nanosheets, and fullerene-like nanoparticles were successfully obtained from rare-earth hydroxides. Their conversions into nanostructures of other rare-earth compounds, functionalization, and optical properties have been demonstrated. The conversion between nanotubes, nanosheets, and nanowires are indicative of the possibilities for the synthesis of nanostructures from other compounds. These synthetic strategies can furthermore be easily adjusted to prepare 1D nanostructures of rare-earth compounds on a large scale. The chemistry and physics in these nanostructures would be interesting, and deserve further and systematical study.

Experimental Section

Chemicals: All the chemicals were of analytical grade and used as received without further purification. Deionized water was used throughout. RE_2O_3 (Y_2O_3, La_2O_3, Pr_2O_3, Nd_2O_3, Sm_2O_3, Eu_2O_3, Gd_2O_3, Th_2O_3, Dy_2O_3, Ho_2O_3, Er_2O_3, Tm_2O_3, Yb_2O_3, purity, >99.99%), NH_4F, HF, NaOH, and HCl (A.R.) were all supplied by Beijing Chemical Reagent Company.

Synthesis of rare-earth hydroxide nanowires and nanotubes: RE_2O_3 (0.4 g) was dissolved in 10% nitric acid, and the pH was then rapidly adjusted to a designated value by using 10% KOH (or NaOH) solution. A white precipitate of amorphous $RE(OH)_3$ appeared immediately. After stirring for about 10 min, the precipitate was then transferred into a 50 mL autoclave, which was filled with deionized water up to 80% of the total volume, sealed, and heated at 120–180 °C for approximately 12 h. The system was then allowed to cool to room temperature. The final product was collected by filtration, and washed with deionized water to remove any possible ionic remnants, and then dried at 60 °C.

Synthesis of hydroxide nanotubes and IF nanoparticles based on a direct oxide conversion method: In a typical synthesis, Ln_2O_3 (La_2O_3, Pr_6O_{11}, Nd_2O_3, Sm_2O_3, Eu_2O_3, Gd_2O_3, Tb_4O_7, Dy_2O_3, Ho_2O_3, Er_2O_3, Y_2O_3, 0.4 g) powder was dispersed into distilled water (30 mL), then sealed into a 40 mL autoclave, and treated at 140–180 °C for 24 hours under hydrothermal conditions. Following this process, hydroxide nanotubes and IF nanoparticles were obtained.

Synthesis of rare-earth fluoride IF nanoparticles: The synthesis of fluoride IF nanoparticles was based on the preparation of a rare-earth fluoride colloidal precipitate and the subsequent hydrothermal treatment at a designated temperature. In a typical synthesis, rare earth oxide (0.4 g, Y_2O_3, La_2O_3, Pr_2O_3, Nd_2O_3, Sm_2O_3) was dissolved in 10% diluted nitric acid and then mixed with another solution containing NH_4F (mole ratio, $Ln^{3+}:F^- = 1:3$) to form colloidal precipitates. 10% KOH (or NaOH) was then added to adjust the pH to a designated value of 4–5. The as-obtained colloidal precipitate was transferred into a 40 mL autoclave, sealed, and kept at 80–180 °C for 12–24 h. By following the above procedure, IF nanoparticles of LaF_3, PrF_3, NdF_3, SmF_3, and YF_3 were easily be obtained. To obtain IF nanostructures with different sizes, several factors (such as mole ratio and temperature) were varied in the experimental procedure. The functionalization process was easily be carried out by dissolving the corresponding rare-earth oxides with target ions or atoms.

Powder X-ray diffraction (XRD): The phase purity of the products was examined by XRD by using a Brucker D8-Advance X-ray diffractometer with $Cu_{K\alpha}$ radiation ($\lambda = 1.5418$ Å), and with the operation voltage and current at 40 kV and 40 mA, respectively. The 2θ range used was from 10 to 70° in steps of 0.02° with a count time of 2 s.

Transmission electron microscopy (TEM): The size and morphology of the products were observed by using a Hitachi Model H-800 transmission electron microscope, with a tungsten filament at an accelerating voltage of 200 kV. Electron diffraction and energy dispersive X-ray analysis were also performed to study the single-crystal nature or elemental composition of the samples. Structural information of the nanocrystals was obtained by high-resolution transmission electron microscopy (HRTEM) on a JEOL JEM-2010F transmission electron microscope operated at 200 kV.

Thermogravimetric analysis (TGA): TGA of the samples were conducted on a TGA-2050 (TA Corp.).

Optical and luminescence measurements: The optical properties and photoluminescence of samples were characterized with a Perkin Elmer LS50B Luminescence Spectrometer operated at room temperature.

Acknowledgement

We thank for Mr. Xiaoming Sun for experimental help. This work was supported by the NSFC (20025102, 50028201, 20151001), the Foundation for the Author of National Excellent Doctoral Dissertation of the P. R. China, and the State Key Project of Fundamental Research for nanomaterials and nanostructures.

[1] W. Tremel, *Angew. Chem.* **1999**, *111*, 2311–2315; *Angew. Chem. Int. Ed* **1999**, *38*, 2175–2179.
[2] J. T. Hu, T. W. Odom, C. M. Lieber, *Acc. Chem. Res.* **1999**, *32*, 435–445.
[3] Y. Y. Wu, H. Q. Yan, M. Huang, B. Messer, J. H. Song, P. D. Yang, *Chem. Eur. J.* **2002**, *8*, 1261–1268.
[4] R. Tenne, *Chem. Eur. J.* **2002**, *8*, 5297–5304.
[5] G. R. Patzke, F. Krumeich, R. Nesper, *Angew. Chem.* **2002**, *114*, 2554- 2571; *Angew. Chem. Int. Ed.* **2002**, *41*, 2446- 2461.
[6] T. J. Trentler, K. M. Hickman, S. C. Goel, A. M. Viano, P. C. Gibbons, W. E. Buhro, *Science* **1995**, *270*, 1791–1794.
[7] T. J. Trentler, S. C. Goel, K. M. Hickman, A. M. Viano, M. Y. Chiang, A. M. Beatty, P. C. Gibbons, W. E. Buhro, *J. Am. Chem. Soc.* **1997**, *119*, 2172–2181.
[8] Y. D. Li, X. F. Duan, Y. T. Qian, L. Yang, M. R. Ji, C. W. Li, *J. Am. Chem. Soc.* **1997**, *119*, 7869–7870.
[9] Y. D. Li, Z. Y. Wang, X. F. Duan, G. H. Zhang, C. Wang, *Adv. Mater.* **2001**, *13*, 145–148.
[10] Y. D. Li, H. W. Liao, Y. Ding, Y. T. Qian, L. Yang, G. E. Zhou, *Chem. Mater.* **1998**, *10*, 2301–2303.
[11] Y. D. Li, H. W. Liao, Y. Ding, Y. Fan, Y. Zhang, Y. T. Qian, *Inorg Chem.* **1999**, *38*, 1382–1387.

[12] Q. Peng, Y. J. Dong, Z. X. Deng, Y. D. Li, *Inorg. Chem.* **2002**, *41*, 5249–5254.
[13] J. P. Ge, Y. D. Li, G. Q. Yang, *Chem. Commun.* **2002**, 1826–1827.
[14] X. F. Duan, C. M. Lieber, *Adv. Mater.* **2000**, *12*, 298–302.
[15] X. G. Peng, M. C. Schlamp, A. V. Kadavanich, A. P. Alivisatos, *J. Am. Chem. Soc.* **1997**, *119*, 7019–7029.
[16] Z. A. Peng, X. G. Peng, *J. Am. Chem. Soc.* **2001**, *123*, 1389 - 1395.
[17] W. W. Yu, X. G. Peng, *Angew. Chem.* **2002**, *114*, 2474–2477; *Angew. Chem. Int. Ed.* **2002**, *41*, 2368–2371.
[18] M. H. Huang, S. Mao, H. Feick, H. Q. Yan, Y. Y. Wu, H. Kind, E. Weber, R. Russo , P. D. Yang, *Science* **2001**, *292*, 1897–1899.
[19] M. Law, H. Kind, B. Messer, F. Kim, P. D. Yang, *Angew. Chem.* **2002**, *114*, 2511–2514; *Angew. Chem. Int. Ed.* **2002**, *41*, 2405–2408.
[20] M. E. Spahr, P. Bitterli, R. Nesper, M. Müller, F. Krumeich, H. U. Nissen, *Angew. Chem.* **1998**, *110*, 1339–1342; *Angew. Chem. Int. Ed.* **1998**, *37*, 1263–1266.
[21] B. Gates, Y. D. Yin, Y. N. Xia, *J. Am. Chem. Soc.* **2000**, *122*, 12582–12583.
[22] X. Wang, Y. D. Li, *J. Am. Chem. Soc.* **2002**, *124*, 2880–2881.
[23] X. Wang, Y. D. Li, *Chem. Eur. J.* **2003**, *9*, 300–306.
[24] X. Wang, Y. D. Li, *Angew. Chem.* **2002**, *114*, 4984–4987; *Angew. Chem. Int. Ed.* **2002**, *41*, 4790–4793.
[25] Y. D. Li, J. W. Wang, Z. X. Deng, Y. Y. Wu, X. M. Sun, D. P. Yu, P. D. Yang, *J. Am. Chem. Soc.* **2001**, *123*, 9904–9905.
[26] X. L. Li, J. F. Liu, Y. D. Li, *Appl. Phys. Lett.* **2002**, *81*, 4832–4834.
[27] Y. Feldman, E. Wasserman, D. J. Srolovitz, R. Tenne, *Science* **1995**, *267*, 222–225.
[28] R. Tenne, L. Margulis, M. Genut, G. Hodes, *Nature* **1992**, *360*, 444–446.
[29] Y. D. Li, X. L. Li, R. R. He, J. Zhu, Z. X. Deng, *J. Am. Chem. Soc.* **2002**, *124*, 1411–1416.
[30] M. Nath, C. N. R. Rao, *Angew. Chem*, **2002**, 114, 3601–3604; *Angew. Chem. Int. Ed.* **2002**, 41, 3451–3454.
[31] Z. W. Pan, Z. R. Dai, Z. L. Wang. *Science* **2001**, *291*, 1947–1950.
[32] X. M. Sun, X. Chen, Y. D. Li, *Inorg. Chem.* **2002**, *41*, 4996–4998.
[33] X. M. Sun, Y. D. Li, *Chem. Eur. J.* **2003**, *9*, 2229–2238.
[34] G. X. Xu, *Rare Earths,* 2nd ed., Metallurgical Industry Press, Beijing, **1995**.
[35] H. Maas, A. Currao, G. Calzaferri, *Angew. Chem.* **2002**, *114*, 2607–2608; *Angew. Chem. Int. Ed.* **2002**, *41*, 2495–2496.
[36] K. L. Frindell, M. H. Bartl, A. Popitsch, G. D. Stucky, *Angew. Chem.* **2002**, *114*, 1001–1004; *Angew. Chem. Int. Ed.* **2002**, *41*, 959–962.
[37] M. Yada, M. Mihara, S. Mouri, M. Kuroki, T. Kijima, *Adv. Mater.* **2002**, *14*, 309–313.
[38] M. Yada, H. Kitamura, A. Ichinose, M. Machida, T. Kijima, *Angew. Chem.* **1999**, *111*, 3716–3720; *Angew. Chem. Int. Ed.* **1999**, *38*, 3506–3510.
[39] X. Wang, X.-M. Sun, D. Yu, B.-S. Zou, Y. D. Li, *Adv. Mater.* **2003**, *15*, 1442–1445; X. Wang, Y. D. Li *Angew. Chem.* **2003**, *115*, 3621–3624; *Angew. Chem. Int. Ed.* **2003**, *42*, 3497–3500.
[40] T. Sasaki, M. Watanabe, H. Hashizume, H. Yamada, H. Nakazawa, *J. Am Chem. Soc.* **1996**, *118*, 8329–8335.

Received: January 29, 2003
Revised: June 30, 2003 [F4785]

